

Observation of two successive quantum supershells in a 15 000-electron fermionic system

M. Pellarin, E. Cottancin, B. Bagueard, J. Lermé, J. L. Vialle, and M. Broyer

*Laboratoire de Spectrométrie Ionique et Moléculaire, CNRS and Université Lyon 1, Bâtiment 205,
43 Boulevard du 11 Novembre 1918, 69622 Villeurbanne Cedex, France*

(Received 7 August 1995)

The electronic shell structure of gallium clusters has been investigated up to nearly 15 000 valence electrons and two successive supershell nodes are observed. The location of these nodes around 2500 and 7500 electrons, respectively, is interpreted in the framework of the jellium model by introducing the ion pseudopotential and a surface softness for the ionic density.

The quantum energy levels of electrons in a spherical potential are highly degenerate due to the spherical symmetry of the problem. In cluster physics, this effect leads to the so-called electronic shell structure.¹ For large sizes, the semiclassical theory shows that the electronic shell structure corresponds to a quantization condition for closed classical orbits of the electron, among which the triangular and square ones are dominant.² They have about the same length and lead practically to the same shell periodicity. However, the small difference in length between these two orbits introduces a phase shift and results in a beating structure which is called a supershell structure. The first supershell node has already been observed in sodium^{3,4} and lithium⁵ clusters around 1000 valence electrons.

Two questions now arise: What is the limitation in size of this electronic shell structure in a real cluster system, and is it possible to observe several quantum supershell nodes when the cluster size increases?

In alkali clusters, the electronic shells were observed up to 2500–3000 electrons^{3–5} while the second supershell node is expected around 4000 electrons. This limitation in size for the observation of electronic shells is probably due to the decrease of the energy gaps between electronic levels as the size increases and to the influence of the temperature, which tends to smear out the oscillations^{5,6} in mass spectra. Unfortunately, if the temperature is lowered below the melting point, the clusters become solid and faceted.⁷ As a consequence, the spherical symmetry will be destroyed and the electronic shells and supershells will no longer exist.

In this paper we report the observation of electronic shells in gallium clusters up to nearly 15 000 electrons with the clear emergence of two successive supershells. Gallium is probably the best candidate for such experiments. It is a trivalent metal with a low Wigner-Seitz radius ($r_s = 2.19$ a.u.) and a very low melting point (303 K). Therefore the energy gaps are larger than in alkali clusters and the cluster symmetry is expected to remain spherical even at low temperature.⁸ In a previous experiment,⁹ we have shown that electronic shells may be clearly observed in mass spectra obtained by near-threshold photoionization. The first supershell node occurs at 2500 electrons, while it was predicted at 1150 electrons in the framework of the standard jellium model.¹⁰ The experi-

mental setup remains almost the same as previously.^{9,11} It has only been improved in order to detect larger clusters. The clusters are produced by the laser vaporization technique. The block source is cooled down to about 100 K by liquid nitrogen to prevent the gallium rod from melting. The clusters are photoionized by a UV laser having a photon energy close to the ionization threshold. They are then analyzed through a Wiley–McLaren time-of-flight (TOF) mass spectrometer perpendicular to the cluster beam. The initial transverse velocity of the clusters in the TOF is compensated by an electric field applied between two deflector plates. With this geometry the mass resolution is good (400 in our case) but the mass range of the spectrometer is limited. For the present study, our interest mainly concerns clusters containing 500–5000 atoms. With our mass spectrometer we cannot expect to resolve individual cluster peaks beyond 500 atoms and the electronic shells will result in intensity oscillations on an unresolved mass spectrum. In the present experiment we need to extend the accessible mass range of the spectrometer. For this purpose, the accelerating voltage of our TOF is increased from 4000 to 6000 V, and a linear ramp voltage is applied to the deflector plates.¹² The length of our TOF is also shortened from 1.30 to 0.8 m. This results first in an improvement to the efficiency because the solid angle of the detector is increased, but also in an enlargement of the accessible mass range on the high mass side: The temporal focusing conditions are such that the first electric field of the TOF (extraction field) must be increased, thus limiting the transverse drift of the cluster ions. Finally, the cluster ions are postaccelerated at 8 kV just before the microchannel plates in order to improve the detector efficiency for larger clusters.¹³

Figure 1 shows typical mass spectra obtained on gallium clusters in the $N = 500$ –5000 size range corresponding to a number N_e of valence electrons from 1500 to 15 000. For each spectrum, the bell-shaped envelope is due to the setting of the mass spectrometer that maximizes the intensity at different mass ranges centered at different mass sizes. The ionization energy is also slightly changed to remain close to the threshold (4.72, 4.68, and 4.63 eV for *A*, *B*, and *C* spectra, respectively). Clear and regular oscillations appear on these spectra. They are related to oscillations in the ionization potential as a func-

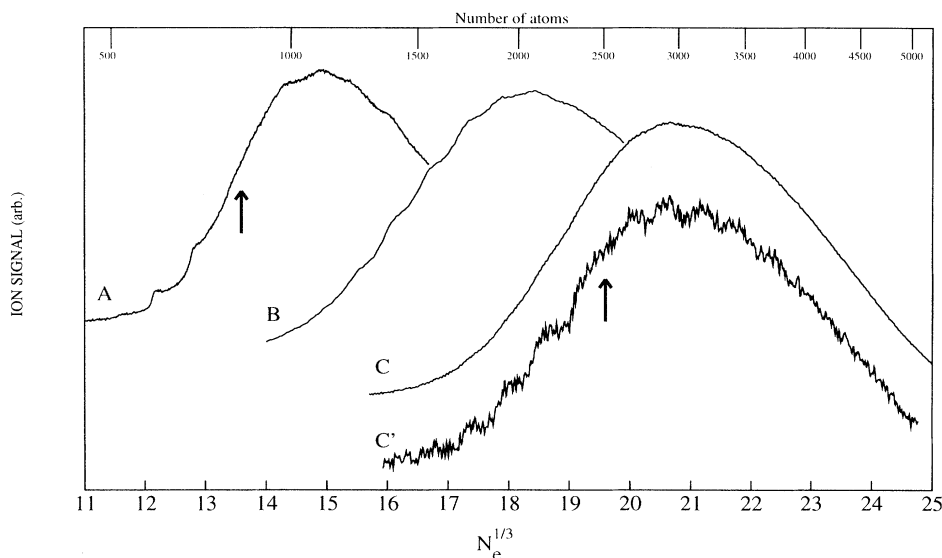


FIG. 1. Three mass spectra of gallium clusters. In each case, the mass range analyzed by the spectrometer is centered at a different mean mass value and the photoionization energy is chosen to be close to the threshold ($h\nu=4.72$, 4.68 , and 4.63 eV for spectra *A*, *B*, and *C*, respectively). Spectrum *C'* is the same as spectrum *C* but part of the bell-shaped envelope has been removed (80%) and the resulting spectrum has been multiplied by a factor of 5. The two node regions of the supershell structure are indicated by arrows.

tion of the size. In spectrum *A*, the oscillation amplitude is modulated by the supershell structure, the first node of which is indicated by an arrow.

As expected, the relative oscillation amplitude decreases with the size. In spectrum *B*, we can see the oscillations between the two supershell nodes. In spectrum *C*, corresponding to the largest clusters, the oscillations remain present, but their amplitude is only on the order of 1% of the signal and they are difficult to see “by the eyes” on the raw spectrum. However, the signal-to-noise ratio is good enough to clearly observe them. In order to amplify the oscillations and to show how they emerge from the spectrum, we have subtracted from the raw signal 80% of the strongly smoothed bell-shaped envelope. Multiplying the resulting signal by 5, we obtain spectrum *C'*. In a way, spectrum *C'* is the same as spectrum *C*, but the noise and oscillations are expanded by a factor of 5. In spectrum *C'*, the oscillations and the second supershell node are clearly visible as in spectrum *A*. This second node is also indicated by an arrow. Spectrum *C* was obtained after averaging the ion signal on about 20 000 laser shots. The signal-to-noise ratio is illustrated by spectrum *C'* where the oscillation, which represents about 1% of maximum intensity, clearly emerges from the noise. Four spectra similar to spectrum *C* have been recorded with slightly different experimental conditions (different ionizing photon energy within 0.01 eV, slightly different delay between the vaporization laser and the ionizing laser etc.). All these spectra show the same reproducible features: minima of the oscillating pattern at the same positions within the error bars (± 0.08 in the $N_e^{1/3}$ scale) and a second node at about $N_e^{1/3} = 19.6$.

In order to quantitatively analyze the signal oscillations, we subtract from the raw signal the strongly smoothed bell-shaped envelope and obtain a so-called difference spectrum which brings to light the oscillations. After a slight smoothing, the oscillating pattern obtained from spectra *A*, *B*, and *C* are shown in Fig. 2. The common vertical scale in Fig. 2 is defined as the ratio, in percentage, between the difference spectrum and the max-

imum of the corresponding raw spectrum. For spectra *B* and *C*, the difference spectra have been multiplied by the factor given in Fig. 2. The figure illustrates roughly the decrease of the oscillation amplitude when the cluster size increases. However, since the *y* scale of the difference spectra is referred to the maximum of the corresponding raw spectra, the true contribution of the oscillating signal is actually much larger in the wings of the detected mass range.

The nodes in the supershell structure are clearly visible in Fig. 2, spectrum *A* and spectrum *C*. In spectrum *B*, the second node occurs in a region where the signal is decreasing and becomes too small to allow the observation of the oscillations beyond the second node. Moreover, the photon energy is also slightly too high in spectrum *B* for the region $20 < N_e^{1/3} < 24$. These nodes are found at about 2500 electrons ($N_e^{1/3} \approx 13.6$) and 7500 electrons ($N_e^{1/3} \approx 19.6$). These results are in disagreement with the standard jellium-model calculations, which predict these nodes at 1150 electrons ($N_e^{1/3} \approx 10.5$) and 4500 electrons ($N_e^{1/3} \approx 16.5$). In previous papers,^{9,14} we have shown that increasing the surface softness of the effective electronic potential may explain this discrepancy. This additional softness has very likely a twofold origin, namely, a softer averaged ionic density at the surface (roughness, large vibrations of the surface atoms)¹⁵ and ion pseudopotential effects.¹⁶ Both ingredients have been taken into account to perform the shell energy calculation presented in Fig. 2. We use the convolution of a trapezoidal ionic distribution (full width at half maximum of the triangular tail equal to 1.5 a.u.) with a local Ascroft-type parametrization of the electron-ion pseudopotential¹⁷ for calculating the total electron-background interaction. The core radius $r_c = 1.17$ a.u. was chosen to ensure the bulk stability at the experimental density $r_s = 2.19$ a.u. and was found to be equal to the Ga^{3+} ion radius tabulated in the literature.¹⁸ This determination involves the bulk energy functional of Ref. 19, with the Coulomb term appropriate to liquid structure and a band-structure term equal to zero. Reliability of this local parameterization is supported by

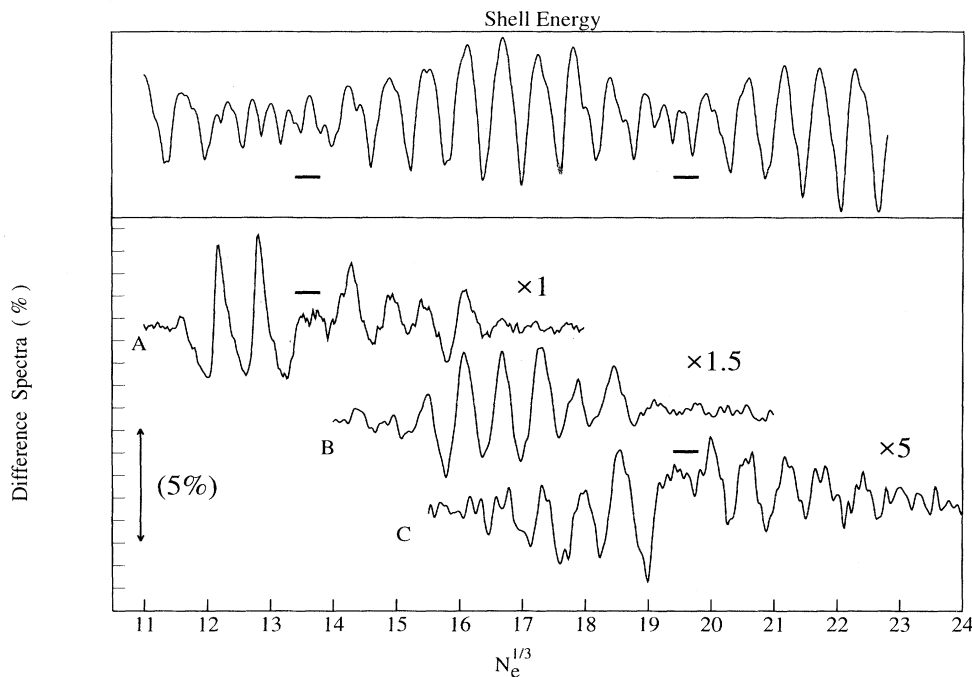


FIG. 2. Upper part: Slightly smoothed theoretical shell correction energy curve for gallium clusters calculated in the framework of the jellium model, including an Ashcroft-type parametrization of the electron-ion-pseudopotential and assuming an inhomogeneous ionic density at the surface (see text). Lower part: Difference spectra for A, B, and C mass spectra of Fig. 1 (see text). The percentage of the oscillations is referred to the maximum intensity of the corresponding raw spectra of Fig. 1. An elementary division corresponds to 1% of the maximum intensity. The two super-shell nodes, as well as the oscillations, are clearly observed.

a very recent calculation showing that, in the case of a step-profile ionic surface distribution and up to the size $N_e = 3000$ valence electrons (upper size limit of the study reported in Ref. 20), the resulting electronic shell structure is identical to the one obtained when using a sophisticated pseudopotential including nonlocal effects.²¹ Let us point out that the triangular shape of the surface ion distribution we considered in our calculation was only assumed for consistency with previous work.⁹ For instance, identical softness effects are obtained from an ion density having a Wood-Saxon curve profile with a thickness parameter on the order of 0.5 a.u. Obviously, owing to the present lack of reliable knowledge of the surface ionic arrangement in large clusters and its dependence versus the experimental conditions, the thickness of the triangular tail of the surface ion density must be considered as a free parameter, and it has been adjusted to obtain an overall agreement with experiment. Let us note that a slight change of the surface softness affects noticeably the node locations only, but not the periodicity of the shell structure (Refs. 9 and 14) nor the number of shells between two nodes. The shell correction energy curve displayed in Fig. 2 is obtained from independent-electron calculations with an effective electronic surface potential fitted on self-consistent Kohn-Sham results carried out on a few large clusters.²²

The agreement obtained between the theoretical calculations and the experimental data in Fig. 2 is quite good; especially the number of shells between the two successive supershell nodes is the same. However, at this point, we must comment on the calibration of our time of flight.

Because of the initial velocity of the clusters and the effects of the electrostatic deflectors, the arrival time t_N for the Ga_N^+ clusters is not related exactly to the effective

length L of the TOF by the simple law $t_N = \sqrt{m/2eV_0} \sqrt{N} L$ where V_0 is the accelerating voltage and m the gallium atomic mass. The effect of the electrostatic deflector is to add the transverse initial kinetic energy $\frac{1}{2} m N v_i^2$ to the electrostatic energy eV_0 . The electrostatic potential is zero before and beyond the deflector, therefore the energy is conserved but the velocity direction has changed. Considering that v_i is roughly independent of the cluster size and equal to the helium velocity, t_N becomes at first order $t_N = \sqrt{m/2eV_0} \sqrt{N} (1 - \beta N)$.

It is impossible to exactly calculate β from experimental parameters because the initial velocity of neutral clusters is not perfectly known. So we get a first approximate value of β from the mass-resolved pattern of the TOF spectrum ($N < 200$) and also from the mass spectra of large aluminum clusters for which the oscillation periodicity due to octahedral symmetry is well known.^{11,23} The final precise determination of β ($\beta = 1.2 \times 10^{-5}$) was obtained by adjusting the third experimental signal dip after the second node ($N_e^{1/3} = 21.5$) to the corresponding theoretical shell closing number. Our initial uncertainty on this β parameter represents only a fraction of the spacing between two shells at $N_e^{1/3} \approx 22$. Our final calibration choice concerns only the last shells in spectrum C and affects neither the location of the two supershell nodes nor the number of shells between the two nodes.

In order to better characterize the phase shift between the shells through the node regions, we plotted the $N_e^{1/3}$ values of the observed minima in experimental spectra as a function of their index k . The results are shown in Fig. 3. Three dashed parallel straight lines corresponding to the curves $N_e^{1/3} = 0.60k + \alpha_i$ with $i = 1, 2, 3$ and

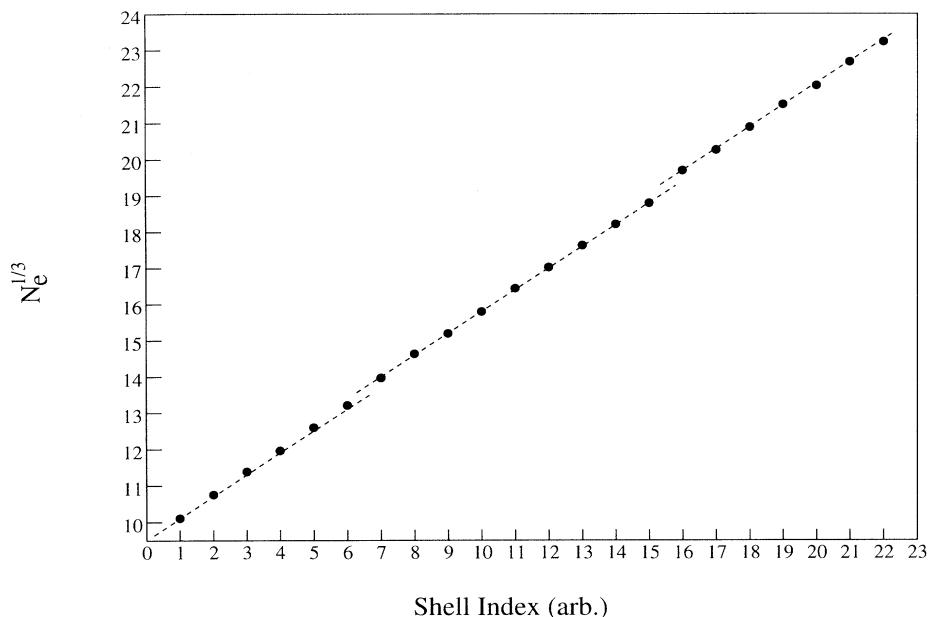


FIG. 3. $N_e^{1/3}$ for the minima in photoionization mass spectra, as a function of the shell index k . The three straight lines are parallel and vertically shifted from each other by $\Delta N_e^{1/3} = 0.3$. This corresponds to a horizontal shift $\Delta k = 0.5$. This figure illustrates the π -phase shift between the shells on each side of a node region.

$\alpha_2 - \alpha_1 = \alpha_3 - \alpha_2 = 0.3$ are in a good agreement with the experimental points. The value of $\alpha_{i+1} - \alpha_i$ (half of the shell period) is necessary for reproducing the π shift in the oscillation phase which occurs through each node in a classical beating structure. α_1 is adjusted on the experimental points. α_1 , as well as the slope 0.60, are in perfect agreement with the set of shell closing numbers deduced from the theory. In fact the parameters that define the three parallel straight lines are not fitted on the experimental points, except α_1 . By changing slightly the slope of these three lines, the phase shift may become slightly different from π . The error bar may be estimated to be $\pm 0.4\pi$. It must be remarked that this phase shift occurs over very few oscillations (two or three). As a consequence, it is not possible to put the experimental points just before and beyond the nodes along a single straight line (with a reasonable slope). Therefore, the two main characteristics of the supershell structure are observed without ambiguity: the modulation of the shell amplitude with nodes and antinodes and a phase shift of the order of π between the shells on each side of a node region.

Is it possible to go further and to study electronic shells for yet larger clusters? As already pointed out, the oscillation amplitude rapidly decreases with the size. As illustrated by Figs. 1 and 2, the total peak-to-peak oscillation amplitude is typically 10% of the signal before the first supershell node, a few percent between the two nodes, and 0.5–1% beyond the second node. We expect that this amplitude drops down to one or two parts per thousand beyond the third node. Therefore, it would be

come very difficult to extract the oscillation signal and to measure the electronic shells. For this, we need to improve the signal-to-noise ratio by a factor of ten at least. In principle it is also possible to cool down the cluster source below the nitrogen liquid temperature, but we cannot be sure that under these conditions the clusters would remain liquid, even if gallium is known to be easily undercooled. The observation of the electronic shell structure for significantly larger cluster sizes is probably possible but not trivial.

In conclusion, electronic shell and supershell structures are obtained in a fermionic system containing up to nearly 15 000 electrons. Two successive supershell nodes are observed. The shell periodicity as a function of $N_e^{1/3}$ is equal, within the experimental uncertainty, to the values measured for alkali clusters,^{3–5} and represents a universal value characteristic of the flat bottom spherical potential ($\Delta N_e^{1/3} \approx 0.6$). Moreover, although the location of the first supershell node depends strongly on the electron-ion pseudopotential and surface properties, the interval between the two first nodes ($\Delta N_e^{1/3} \approx 6$) is also independent of the element as illustrated by our theoretical and experimental results.

We want to thank C. Clavier, G. Guiraud, and F. Valadier for valuable technical assistance, and P. Melinon and C. Bordas for very helpful and stimulating discussions. T. P. Martin is also acknowledged for pertinent suggestions and advice.

- ¹W. D. Knight, K. Clemenger, W. A. de Heer, W. A. Saunders, M. Y. Chou, and M. L. Cohen, *Phys. Rev. Lett.* **52**, 2141 (1984).
- ²R. Balian and C. Bloch, *Ann. Phys.* **69**, 76 (1971); M. V. Berry and M. Tabor, *Proc. R. Soc. London Ser. A* **356**, 375 (1977).
- ³J. Pedersen, S. Bjørnholm, J. Borggreen, K. Hansen, T. P. Martin, and H. D. Rasmussen, *Nature* **353**, 733 (1991).
- ⁴T. P. Martin, S. Bjørnholm, J. Borggreen, C. Bréchnignac, Ph. Cahuzac, K. Hansen, and J. Pedersen, *Chem. Phys. Lett.* **186**, 53 (1991).
- ⁵C. Bréchnignac, Ph. Cahuzac, F. Carlier, M. de Frutos, and J. Ph. Roux, *Phys. Rev. B* **47**, 2271 (1993).
- ⁶O. Genzken and M. Brack, *Phys. Rev. Lett.* **67**, 3286 (1991).
- ⁷T. P. Martin, T. Bergmann, H. Göhlich, and T. Lange, *Chem. Phys. Lett.* **172**, 209 (1990).
- ⁸P. Stampfli and K. H. Bennemann, *Phys. Rev. Lett.* **69**, 3471 (1992).
- ⁹M. Pellarin, B. Baguenard, Ch. Bordas, M. Broyer, J. Lermé, and J. L. Vialle, *Phys. Rev. B* **48**, 17 645 (1993).
- ¹⁰O. Genzken, M. Brack, E. Chabanat, and J. Meyer, *Ber. Bunsenges. Phys. Chem.* **96**, 1217 (1992).
- ¹¹M. Pellarin, B. Baguenard, M. Broyer, J. Lermé, J. L. Vialle, and A. Perez, *J. Chem. Phys.* **98**, 944 (1993).
- ¹²W. A. de Heer and P. Milani, *Rev. Sci. Instrum.* **62**, 670 (1991).
- ¹³V. Zimmermann, N. Malinowski, V. Näher, S. Franck, and T. P. Martin, *Z. Phys. D* **31**, 85 (1994).
- ¹⁴J. Lermé, Ch. Bordas, M. Pellarin, B. Baguenard, J. L. Vialle, and M. Broyer, *Phys. Rev. B* **48**, 12 110 (1993).
- ¹⁵H. P. Cheng and R. S. Berry, *Phys. Rev. A* **45**, 7969 (1992).
- ¹⁶J. Lermé, M. Pellarin, B. Baguenard, C. Bordas, J. L. Vialle, and M. Broyer, *Phys. Rev. B* **50**, 5558 (1994).
- ¹⁷N. W. Aschroft, *Phys. Lett.* **23**, 48 (1966).
- ¹⁸*Handbook of Chemistry and Physics*, 71st ed. (CRC, Boca Raton, FL, 1990), p. 12.1.
- ¹⁹N. W. Aschroft and D. C. Langreth, *Phys. Rev.* **155**, 682 (1967).
- ²⁰J. Lermé, M. Pellarin, J. L. Vialle, and M. Broyer, *Phys. Rev. B* **52**, 2868 (1995).
- ²¹G. B. Bachelet, D. M. Ceperley, and M. G. B. Chiochetti, *Phys. Rev. Lett.* **62**, 2088 (1989).
- ²²J. Lermé, Ch. Bordas, B. Baguenard, M. Pellarin, J. L. Vialle, and M. Broyer, *Phys. Rev. B* **48**, 9028 (1993).
- ²³T. P. Martin, U. Näher, and H. Schaber, *Chem. Phys. Lett.* **199**, 470 (1992).